

Growth, Characterization, Vortex Pinning and Vortex Flow Properties of Single Crystals of Iron Chalcogenide Superconductor $\text{FeCr}_{0.02}\text{Se}$

Anil K. Yadav¹, Ajay D. Thakur² *, C. V. Tomy¹ †

¹ *Department of Physics, Indian Institute of Technology Bombay, Mumbai 400076, India*

² *School of Basic Sciences, Indian Institute of Technology Patna, Patna 800013, India*

(Dated: December 5, 2012)

Abstract

We report the growth and characterization of single crystals of iron chalcogenide superconductor $\text{FeCr}_{0.02}\text{Se}$. There is an enhancement of the superconducting transition temperature (T_c) as compared to the single crystal of the parent compound Fe_{1+x}Se by about 25%. The superconducting parameters such as the critical fields, coherence length, penetration depth and the Ginzburg-Landau parameter have been estimated for these single crystals and compared with related Fe-based superconductors. Analysis of the critical current data suggests a δl pinning mechanism in this material. Thermally activated transport across the superconducting transition in the presence of external magnetic field suggest a crossover from a single vortex pinning regime at low fields to a collective flux creep regime at higher magnetic fields. Nature of charge carriers in the normal state estimated from Hall effect and thermal transport measurements could provide crucial information on the mechanism of superconductivity in Fe-based materials.

PACS numbers: 74.25.Dw, 74.70.Xa

* Corresponding Author

Email: ajay.thakur@iitp.ac.in

† Corresponding Author

Email: tomy@phy.iitb.ac.in

Iron chalcogenide α -FeSe crystallizes in the hexagonal NiAs type crystal structure with $P6_3/mmc$ space group, and is non-superconducting. A slight excess of Fe stabilizes the superconducting tetragonal phase β -Fe $_{1+x}$ Se (anti-PbO type; space group $P4/nmm$) with a superconducting transition temperature (T_c) of ~ 8.5 K [1]. FeSe and its derivatives (commonly known as the ‘11’ system among the Iron based superconductors) have drawn immense attention [2, 3] akin to the remarkable similarity in their Fermi surface with that of the FeAs based iron pnictide superconductors [4]. Therefore, despite their structural and compositional simplicity compared to the pnictide counterparts, they are conceived to be promising model systems to understand the physics of Fe-based superconductors. Structurally, FeSe comprises of stacked layers of corner sharing FeSe $_4$ tetrahedra similar to the FeAs based materials. However, the spacer layers are absent. Analogous to the members of the pnictide family, there is a distortion in the FeSe layers across the structural transition. The properties of off-stoichiometric β -Fe $_{1+x}$ Se (or, β -FeSe $_{1-x}$) was observed to be very sensitive to the ambient pressure. Whereas, Mizuguchi *et al.* [5] reported a T_c of 27 K at 1.48 GPa in β -Fe $_{1+x}$ Se, Medvedev *et al.* [6] found a non-monotonicity in the evolution of T_c with pressure with a maximum of 36 K at 8.9 GPa. The T_c was seen to decrease within the pressure range 8.9-32 GPa. A non-monotonic variation of T_c was also observed in the high pressure studies by Margadonna *et al.* [7] where T_c was seen to peak at 37 K at 7 GPa. Garbarino *et al.* [8] on the other hand showed a monotonic increase in T_c with pressure, where, an orthorhombic high pressure phase was seen to develop at 12 GPa with a T_c of 34 K at 22 GPa. Although the precise nature of the superconducting phase and the exact role played by external pressure is not very clear, the sensitive dependence of T_c on ambient pressure suggests a possibility of increasing T_c via the chemical pressure route. Several groups around the world have tried different substitutions at both the Se site [9, 10] and the Fe site [12–14] however, there have been no reports suggesting an enhancement of T_c . Upon Ni substitution at the Fe site, the superconducting volume fraction was seen to enhance, but there was no concomitant increase in T_c [12]. We have recently reported a route to enhancement of T_c by the substitution of Cr instead of excess iron in polycrystalline FeCr $_x$ Se samples [16–18]. We have now been successful in growing single crystals of FeCr $_{0.02}$ Se. In this paper, we report the detailed superconducting and transport properties in these single crystalline samples.

The single crystals used in this work were prepared using the self flux method for crystal

growth. Powders of 4N Fe, Se and Cr obtained from Alfa Aesar were homogenized in an agate mortar in the required stoichiometric composition ($\text{FeCr}_{0.02}\text{Se}$), sealed in an evacuated quartz tube (10^{-6} mbar) and preheated at 1050°C for 24 h. It was cooled down to 800°C at a rate of $2^\circ\text{C}/\text{h}$ and then the furnace was switched off. The sample thus obtained was annealed at 360°C for 36 h followed by quenching in liquid N_2 . The X-ray diffraction (XRD) and energy dispersive X-ray analysis (EDXA) were performed to confirm the structure and elemental composition. Magnetization measurements were performed using the SQUID-Vibrating Sample Magnetometer (SVSM), Quantum Design Inc. (U.S.A.). Electrical and thermal transports were performed using the Physical Property Measurement System (PPMS), Quantum Design Inc. (U.S.A.). The scan amplitude was chosen to be 2.0 mm and 1.0 mm for the PPMS-VSM and SQUID-VSM, respectively.

The single crystals of $\text{FeCr}_{0.02}\text{Se}$ reported in this paper have layered planes held together by weak van der Waals interaction and can therefore be cleaved easily similar to the $\text{FeSe}_{1-x}\text{Te}_x$ [19], NbSe_2 [20–22] and Bi-2212 [23, 24] single crystals. The X-ray diffraction pattern obtained for one such cleaved single crystal piece is shown in the inset panel of Fig. 1 (a). Prominent (101) reflections are observed indicating that the (101)-axis of the single crystal is perpendicular to the cleaved surface. The panel (a) of Fig. 1 shows the temperature variation of the real part of AC susceptibility data. The onset temperature for the diamagnetic transition is marked as $T_c^{on; dia}$. In panel (b) of Fig. 1, we present a comparison of the DC magnetization and the electrical transport measurements across the superconducting transition in $\text{FeCr}_{0.02}\text{Se}$. Also marked in Fig. 1 (b) are the onset ($T_c^{on} = 14.8\text{ K}$), mid-point ($T_c^{mid} = 12.2\text{ K}$), offset temperatures ($T_c^{off} = 11.1\text{ K}$) and zero resistance temperature ($T_c^0 = 10.5\text{ K}$) which are respectively the temperatures at which ρ reaches 90%, 50%, 10% and 0% of the normal state value (ρ_N) measured in the absence of an external magnetic field ($H = 0$). The temperatures for the onset of diamagnetism ($T_c^{on; dia}$) and zero resistance (T_c^0) coincide with each other (hallmark of superconductivity). This temperature is identified as the superconducting transition temperature (T_c) and has a value of 10.5 K for our crystals of $\text{FeCr}_{0.02}\text{Se}$.

Any practical application of a typical type II superconductor demands an understanding of its vortex phase diagram [25]. In particular, it is of utmost importance to obtain the lower critical field, H_{c1} and the upper critical field, H_{c2} values at various temperatures below T_c . In panels (a) and (b) of Fig.2 we present the H_{c2} data obtained from the electrical transport

data via the magnetic field dependence of the T_c^{on} , T_c^{mid} and T_c^{off} values (see Fig. 1(b)) for both $H \parallel (101)$ and $H \perp (101)$. The value of the slope ($\frac{dH_{c2}}{dT}$) are extracted from graph as -23 kOe/K, -26 kOe/K and -25 kOe/K, for data corresponding to T_c^{on} , T_c^{mid} and T_c^{off} (identical within the first decimal place for both $H \parallel (101)$ and $H \perp (101)$), respectively. The upper critical field values at zero temperatures $H_{c2}(0)$ are therefore estimated as 24 kOe, 22 kOe and 17.5 kOe (for both $H \parallel (101)$ and $H \perp (101)$) using Werthamer-Helfand-Hohenberg (WHH) formalism [26], where, $H_{c2}(0) = -0.693 \left(\frac{dH_{c2}}{dT} \right) T_c$ for the three different criteria, respectively. This points to an absence of magnetocrystalline anisotropy in single crystals of $\text{FeCr}_{0.02}\text{Se}$. The estimated values for $H_{c2}(0)$ are very close to the Pauli paramagnetic limit $H_P(0) = 1.84T_c$ [27], suggesting spin-paramagnetic effect as the dominant pair breaking mechanism similar to the claims made for the FeSe system with S and Te substituted at the Se site [9, 10]. An estimate of the superconducting coherence length $\xi(0)$ was made using the Ginzburg-Landau expression $H_{c2}(0) = \Phi_0/2\pi\xi^2(0)$. The values for $\xi(0)$ was obtained as 1.68 nm, 3.87 nm and 4.33 nm from the plots obtained for T_c^{on} , T_c^{mid} and T_c^{off} , respectively. In order to make an estimate of the lower critical field, H_{c1} , the virgin curves (corresponding to the isothermal M-H measurements) were obtained after zero field cooling. The criteria of deviation from linearity within virgin M-H plots was used to determine H_{c1} . In Fig. 3, we plot the H_{c1} data for both $H \parallel (101)$ and $H \perp (101)$. A BCS fit [28] yields a $H_{c1}(0)$ of 67 Oe and 33 Oe for $H \parallel (101)$ and $H \perp (101)$, respectively. The values of penetration depth $\lambda(0)$, Ginzburg-Landau parameter $\kappa(0)$ along with the critical fields are tabulated in Table I for $\text{FeCr}_{0.02}\text{Se}$. A comparison is made with the superconducting parameters of related Fe-based superconductors. It should be noted here that the BCS fit is not very good at temperatures close to $T_c(0)$ where the experimental data shows a curvature reminiscent of multi-band superconductors.

In case of type-II superconductors, it is feasible to obtain a practical estimate of the critical current density (J_c) via suitable magnetization measurements [29, 30]. This is useful when the contact resistance in a typical magneto-transport measurement is such that passing large currents through the sample for estimation of J_c is impractical without resorting to special protocols [21] for making contacts on the sample. In our case we resort to the contactless technique via magnetization measurements for determination of $J_c(H, T)$ within Bean's model [29, 30]. Typical five quadrant isothermal magnetization hysteresis (M - H) loops recorded at several temperatures between 2 K and 8 K (data at other temperatures not

shown here for clarity) are shown in Fig. 4(a) (for $H \parallel (101)$) and Fig. 4(b) (for $H \perp (101)$). The peak in magnetization located at a field value little above nominal zero field in a given M - H loop represents the first magnetization peak characteristic, which amounts to (near) full penetration of the applied field in the bulk of the sample after zero field cooling. We do not observe any prominent feature corresponding to fishtail effect/second magnetization peak in our crystals. The absence of a magnetocrystalline anisotropy is evident here too (see Fig. 2, where, the values of H_{c2} for both $H \parallel (101)$ and $H \perp (101)$ are presented).

Making use of the Bean's critical state model formalism [29, 30], we extracted critical current density values from the isothermal M - H data. Within Bean's model, $J_c = 20 \frac{\Delta M}{a(1-\frac{a}{3b})}$ [30], with a ($= xx \text{ mm}$) and b ($= yy \text{ mm}$) being the sample dimensions perpendicular to the field direction, and ΔM is the difference between the magnetization measured during the return and the forward legs of the M - H loop. Figure 5 shows the plot of the critical current density $J_c(H)$ at temperatures between 2 K and 10 K for both $H \parallel (101)$ (panel (a)) and $H \perp (101)$ (panel (b)).

Vortex pinning in type-II superconductors can be broadly classified into two categories, viz., δT_c pinning (arising because of the spatial fluctuations in the transition temperature, T_c across the sample) and δl pinning (caused by the spatial variations in the charge carrier mean free path, l). In the case of δT_c pinning, the normalized critical current density, $J_c(t)/J_c(0) = (1 - t^2)^{7/6}(1 + t^2)^{5/6}$, while for δl pinning, $J_c(t)/J_c(0) = (1 - t^2)^{5/2}(1 + t^2)^{-1/2}$, where $t = T/T_c(0)$ [31, 32]. Following a recipe similar to Das *et al* [19] and Thakur *et al* [33, 34], in Fig. 6, we make a comparison of the experimentally obtained J_c values (for $H \parallel (101)$) with the theoretically expected variations within the δT_c and δl pinning scenarios. The observations point to the dominance of the δl pinning mechanism in $\text{FeCr}_{0.02}\text{Se}$, suggesting the occurrence of single vortex pinning by randomly distributed weak pinning centers.

In the presence of an external magnetic field, the dissipation behavior of a typical type-II superconductor is guided by the competition between the pinning force (due to δl or, δT_c pinning) and the Lorentz force (acting on the flux line because of the transport current). The dissipation behavior comprises of two distinct regimes: (a) the pinning force dominated flux-creep regime, and (b) the Lorentz force dominated flux-flow regime. In the case of high T_c superconductor $\text{Bi}_{2.2}\text{Sr}_2\text{Ca}_{0.8}\text{Cu}_2\text{O}_8$, Palstra *et al* [35, 36] conceived of a dissipation behavior guided uniquely by an orientation and field dependent activation energy $U_0(H, \phi)$. It is of interest to evaluate the extent to which such a formalism is applicable for the Fe-

based superconductors. The main panel in Fig. 7 shows the variation of resistivity (ρ) as a function of temperature for a suitably cleaved single crystal of FeCr_xSe at 0 T and 9 T ($\parallel (101)$). The inset panel (a) shows the variation of $\frac{d\rho}{dT}$ with temperature whereas in inset panel (b) is plotted the variation of ρ (close to the superconducting transition) as a function of temperature for $H \parallel (101)$ and $H \perp (101)$, respectively. In order to obtain the activation energy U_0 , in Fig. 8, we plot $\ln \rho$ versus $1/T$ at various fields H for both $H \parallel (101)$ (panel (a)) and $H \perp (101)$ (panel (b)). Linear fits are performed on the low temperature part (large $1/T$ behavior) and these are shown by solid lines in both the panels of Fig. 8. The slopes obtained from these fits yield the values of the activation energies U_0 at various field values for both $H \parallel (101)$ and $H \perp (101)$. As we know, for thermally activated flux-flow behavior, $\ln \rho(T, H) = \ln \rho_0(H) - U_0(H)/T$ [35]. The plots of $\ln \rho$ versus $1/T$ at various fields have a common intersection point (see panels (a) and (b) of Fig. 8) which should ideally correspond to the T_c of the superconducting single crystal. In our case this point corresponds to a $1/T$ value of ≈ 0.078 . This corresponds to a temperature of 12.8 K which is indeed very close to the T_c^{mid} for our single crystals of $\text{FeCr}_{0.02}\text{Se}$. The variation of U_0 with H (for both $H \parallel (101)$ and $H \perp (101)$) is shown in Fig. 9. We find very similar behavior for both the field orientations. Power law fits ($\sim H^{-\alpha}$) are performed on the $U_0(H)$ data and two regimes are clearly evident with a crossover occurring at a characteristic field H_{cross} ($\approx 38 \text{ kOe}$) for both $H \parallel (101)$ and $H \perp (101)$. The values for the exponent α in the two field regions for different field orientations are provided in Table 2. It should be noted here that a similar analysis for $\text{Bi}_{2.2}\text{Sr}_2\text{Ca}_{0.8}\text{Cu}_2\text{O}_8$ by Palstra *et al* [35, 36] also yielded a similar crossover field behavior with different values of α on the two sides. However, in their case, very different values for α were obtained for the two field orientations (possibly related to the large anisotropy in single crystals of $\text{Bi}_{2.2}\text{Sr}_2\text{Ca}_{0.8}\text{Cu}_2\text{O}_8$). Recently, Lei *et al* [37] have found a similar behavior for single crystals of $\beta\text{-FeSe}$ with $H_{cross} \approx 30 \text{ kOe}$ (smaller than the crossover field of $\approx 38 \text{ kOe}$ observed in our single crystals). In the case of $\beta\text{-FeSe}$, $\alpha \approx 0.25$ for $H < H_{cross}$ while for $H > H_{cross}$, $\alpha \approx 0.68$ ($H \parallel (101)$). The values of α for the other field orientation ($H \perp (101)$) were seen to be within few percent of the values for $H \parallel (101)$. In our single crystals of Cr substituted $\beta\text{-FeSe}$, we observe a very similar behavior except that the values of α are marginally larger. This is understandable considering $\approx 30\%$ enhancement in T_c upon 2% Cr substitution at the excess Fe site in $\beta\text{-FeSe}$. A change in the value of the exponent α by about a factor of 3 across H_{cross} with a relatively small value at low fields suggests a

crossover from a single-vortex pinning dominated regime to a collective flux creep regime across H_{cross} [38].

The nature of charge carriers in the normal state just prior to the superconducting transition is one of the crucial ingredients that is required to physically understand the mechanism of superconductivity in any material system. In order to develop an understanding in this direction, we perform both Hall effect studies and the thermal transport measurements (including the determination of Seebeck coefficient (S)) as a function of temperature in a single crystal piece of $\text{FeCr}_{0.02}\text{Se}$. For the Hall measurements, a single crystal piece of $\text{FeCr}_{0.02}\text{Se}$ was mounted on the measurement puck and then repeatedly cleaved using a scotch tape to thin down the specimen. Contacts for the Hall measurements were made in the five probe geometry using silver epoxy and 30 micron gold wires. The observed Hall coefficient as a function of temperature is shown in panel (a) of Fig. 10. From the data it is evident that the Hall coefficient is negative below 220 K pointing to a prominence of electron like charge carriers in this region. Fig. 10 (c) shows a plot of $S(T)$ at external magnetic field values of 0 T and 5 T, respectively. Below the superconducting transition temperature $S(T)$ is zero as the charge carriers are involved in the formation of Cooper pairs. The inset panel in Fig. 10 (c) shows the enlarged view of the $S(T)$ data between 2 K to 20 K. It should be noted that the $S(T)$ measurements confirms the T_c of the sample of 10.5 K as obtained from the magnetization and electrical transport studies (c.f., Fig. 1). In the presence of an external field of 5 T, the shifting of T_c to the lower temperatures is also evident from the $S(T)$ data. Above T_c , $S(T)$ has a positive value and it crosses zero at ~ 65 K. This change of sign is not seen in Hall measurements. Above 65 K the $S(T)$ changes sign and become negative and attains maximum magnitude of $\sim 26 \mu\text{V/K}$ at 109 K. The $S(T)$ data above 109 K suggests a change in the type of majority charge carriers. The change in the type of charge carrier at this temperature is also observed in the Hall measurement. Thus, from the $S(T)$ data, it is clearly evident that this material has both types of charge carriers. A modulation in the fraction of the two types of charge carriers as a function of temperature is responsible for the non-monotonic variations in $S(T)$. This could be crucial information in theoretically understanding the nature of superconducting state in this class of materials.

To summarize, we have grown single crystals of tetragonal phase of $\text{FeCr}_{0.02}\text{Se}$ (anti-PbO type; space group $P4/nmm$) where, 2% Cr is substituted in excess at the Fe site. These single crystals have a T_c which is 30 % larger than the parent $\beta\text{-FeSe}$. The basic superconducting

properties are corroborated using magnetic susceptibility (both AC and DC) as well as electrical transport measurements. An estimate of J_c is obtained using isothermal M - H data which is also utilized to establish the nature of pinning mechanism in these single crystals. A one-to-one comparison between the experimentally obtained temperature variation of J_c with the corresponding theoretical estimates for δl pinning and δT_c pinning is performed. Based on this, the pinning properties within these single crystals are attributed to the δl pinning mechanism which corresponds to the occurrence of single vortex pinning by randomly distributed weak pinning centers. From low field magnetization measurements and magneto-transport studies, fundamental parameters like H_{c1} , H_{c2} , κ , $\xi(0)$, $\lambda(0)$ are obtained which are fundamental to the understanding of magnetic properties of these single crystals. An attempt is made to understand the flux-flow behavior in these single crystals within the thermally activated flux-flow model. The results points to a crossover from single-vortex pinning dominated regime to a collective flux creep regime across a characteristic field H_{cross} [38] which is practically independent of the magnetic field orientation direction. Finally, the issue of nature of charge carriers in the normal state of these single crystals is addressed. For this, we resort to Hall effect, thermopower and thermal conductivity measurements which together suggests a modulation in the fraction of the two types of charge carriers with temperature within the normal state. This could prove to be a vital input for theoretically understanding the nature of the normal state within these class of superconductors and possibly the physics of the mechanism of superconductivity in these systems.

CVT would like to acknowledge the Department of Science and Technology for partial support through the project IR/S2/PU-10/2006. AKY would like to thank CSIR, India for SRF grant. ADT acknowledges the Indian Institute of Technology, Bombay for partial financial support during part of this work and the Indian Institute of Technology, Patna for seed grant.

-
- [1] F. C. Hsu, J. Y. Luo, K. W. Yeh, T. K. Chen, T. W. Huang, P. M. Wu, Y. C. Lee, Y. L. Huang, Y. Y. Chu, D.C. Yan, and M.K. Wu, Proc. Natl. Acad. Sci. (USA) **105**, 14262 (2008).
 - [2] M.K. Wu, F.C. Hsu, K.W. Yeh, T.W. Huang, J.Y. Luo, M.J. Wang, H.H. Chang, T.K. Chen, S.M. Rao, B.H. Mok, C.L. Chen, Y.L. Huang, C.T. Ke, P.M. Wu, A.M. Chang, C.T. Wu,

- T.P. Perng, Physica C **469**, 340 (2009).
- [3] K. Tanabe, Y. Hosono, Jpn. J. of Appl. Phys. 51, 010005 (2012)
 - [4] A. Subedi, L. Zhang, D. J. Singh, and M. H. Du, Phys. Rev. B **78**, 134514 (2008).
 - [5] Y. Mizuguchi, F. Tomioka, S. Tsuda, T. Yamaguchi, Y. Takano, Appl. Phys. Lett. **91**, 152505 (2008).
 - [6] S. Medvedev, T.M. McQueen, I. Trojan, T. Palasyuk, M.I. Eremets, R.J. Cava, S. Naghavi, F. Casper, V. Ksenofontov, G. Wortmann, C. Felser, Nature Materials **8**, 630 (2009).
 - [7] S. Margadonna, Y. Takabayashi, Y. Ohishi, Y. Mizuguchi, Y. Takano, T. Kagayama, T. Nakagawa, M. Takata, and, K. Prassides, Phys. Rev. B **80**, 064506 (2009).
 - [8] G. Garbarino, A. Sow, P. Lejay, A. Sulpice, P. Toulemonde, M. Mezouar, M. Nez-Regueiro, Eur. Phys. Lett. 86 (2009) 27001.
 - [9] K.W. Yeh, Z.W. Huang, Y.L. Huang, T.K. Chen, F.C. Hsu, P.M. Wu, Y.C. Lee, Y.Y. Chu, C.L. Chen, J.Y. Luo, D.C. Yan, M.K. Wu, Europhys. Lett. **84**, 37002 (2008).
 - [10] M.H. Fang, H.M. Pham, B. Qian, T.J. Liu, E.K. Vehstedt, Y. Liu, L. Spinu, Z.Q. Mao, Phys. Rev. B, **78**, 224503 (2008).
 - [11] Y. Mizuguchi, F. Tomioka, S. Tsuda, T. Yamaguchi, Y. Takano, (2008), arxiv:/0811.1123v1.
 - [12] M.K. Wu, F.C. Hsu, K.W. Yeh, T.W. Huang, J.Y. Luo, M.J. Wang, H.H. Chang, T.K. Chen, S.M. Rao, B.H. Mok, C.L. Chen, Y.L. Huang, C.T. Ke, P.M. Wu, A.M. Chang, C.T. Wu, T.P. Perng, Physica C 469 (2009) 340.
 - [13] Y. Mizuguchi, F. Tomioka, S. Tsuda, T. Yamaguchi, Y. Takano, J. Phys. Soc. Japan **78**, 074712 (2009).
 - [14] D.J. Gawryluka, J. Fink-Finowickia, A. Wisniewskia, R. Puzniaka, V. Domukhovskia, R. Diduszkia, b, M. Kozlowskia, M. Berkowskia, arXiv:condmat/1010.4217.
 - [15] A. Gnther, J. Deisenhofer, Ch. Kant, H.-A. Krug von Nidda, V. Tsurkan, A. Loidl, arXiv:condmat/1010.5597.
 - [16] A. K. Yadav, A. D. Thakur, C. V. Tomy, Sol. St. Comm. **151**, 557 (2011).
 - [17] A. K. Yadav, A. D. Thakur, C. V. Tomy, AIP Conf. Proc. 1447, 907 (2012).
 - [18] A. K. Yadav, A. D. Thakur, C. V. Tomy, AIP Conf. Proc. (2013) to be published.
 - [19] P. Das, Ajay D. Thakur, Anil K. Yadav, C. V. Tomy, M. R. Lees, G. Balakrishnan, S. Ramakrishnan, and A. K. Grover, Phys. Rev. B **84**, 214526 (2011).
 - [20] Y. Paltiel, D. T. Fuchs, E. Zeldov Y. N. Myasoedov, H. Shtrikman, M. L. Rappaport, and E.

- Andrei, Phys. Rev. B **58**, R14763 (1998).
- [21] Z. L. Xiao, O. Dogru, E. Y. Andrei, P. Shuk, M. Greenblatt, Phys. Rev. Lett. **92**, 227004 (2004).
 - [22] A. D. Thakur, T. V. Chandrasekhar Rao, S. Uji, T. Terashima, M. J. Higgins, S. Ramakrishnan, A. K. Grover, J. of the Phys. Soc. of Jpn. **75**, 74718 (2006).
 - [23] S. Ooi, T. Mochiku, K. Hirata, Phys. Rev. Lett. **89**, 247002 (2002).
 - [24] S. F. W. R. Rycroft, R. A. Doyle, D. T. Fuchs, E. Zeldov, R. J. Drost, P. H. Kes, T. Tamegai, S. Ooi, and D. T. Foord, Phys. Rev. B **60**, R757 (1999).
 - [25] Y. Ma, Sup. Sci. and Technol. **25**, 113001 (2012)
 - [26] N. R. Werthamer, E. Helfand, and P. C. Hohenberg, Phys. Rev. B **147**, 295 (1966).
 - [27] A. M. Clogston, Phys. Rev. Lett. **9**, 266 (1962).
 - [28] J. Bardeen, L. N. Cooper, J. R. Schrieffer, Phys. Rev. **106**, 162 (1957).
 - [29] C. P. Bean, Rev. Mod. Phys. **36**, 31 (1964).
 - [30] C. P. Poole Jr., H. A. Farach, R. J. Creswick, R. Prozorov, Superconductivity, Second edition (2007), Academic Press.
 - [31] G. Blatter, M. V. Feigel'man, V. B. Geshkenbein, A. I. Larkin, and V. M. Vinokur, Rev. Mod. Phys. **66**, 1125 (1994).
 - [32] R. Greissen, Wen Hai-hu, A. J. J. van Dalen, B. Dam, J. Rector, H. G. Schnack, S. Libbrecht, E. Osquiguil, and Y. Bruynseraede, Phys. Rev. Lett. **72**, 1910 (1994).
 - [33] Ajay D Thakur, Anil K Yadav, P Das, CV Tomy, MR Lees, G Balakrishnan, S Ramakrishnan, AK Grover, AIP Conf. Proc. **144**, 897 (2012).
 - [34] Ajay. D. Thakur, A. K. Yadav, A. Thamizhavel, C. V. Tomy, S. Ramakrishnan and A. K. Grover, AIP Conf. Proc. to be published (2013).
 - [35] T. T. M. Palstra, B. Batlogg, L. F. Schneemeyer, and J. V. Waszczak, Phys. Rev. Lett. **61**, 1662 (1990).
 - [36] T. T. M. Palstra, B. Batlogg, R. B. van Dover, L. F. Schneemeyer, and J. V. Waszczak, Phys. Rev. B **41**, 6621 (1990).
 - [37] H. Lei, R. Hu, C. Petrovic, Phys. Rev. B **84**, 014520 (2011).
 - [38] Y. Yeshurun and A. P. Malozemoff, Phys. Rev. Lett. **60**, 2202 (1988).
 - [39] H-S. Lee, M. Bartkowiak, J. S. Kim, H-J. Lee, Phys. Rev. B **82**, 104523 (2010).

TABLE I: Comparison of superconducting parameters of the single crystal of $\text{FeCr}_{0.02}\text{Se}$ with other related compounds.

Compounds	T_c	H_{c1} (Oe)	H_{c2} (kOe)	ξ (nm)	λ (nm)	κ	anisotropy
$\text{FeCr}_{0.02}\text{Se}$ ($H \parallel (101)$)	10.5	66	220	3.87	334	86.3	Isotropic
$\beta\text{-FeSe}$	8.5	75(1)	180	4.28	~ 309	72.3	Isotropic
$\text{FeSe}_{1-x}\text{Te}_x$	14	< 100	650	2.2	560	254	3.1(2)
$\text{FeTe}_{0.8}\text{S}_{0.2}$	8.4	-	440	2.7	-	-	1.05(4)

TABLE II: Power law decay of activation energy ($U_0 \sim H^{-\alpha}$).

Sample	Field Orientation	H_{cross} (kOe)	α	
			$(H < H_{cross})$	$(H > H_{cross})$
$\text{FeCr}_{0.02}\text{Se}$	$\parallel (101)$	39.3	0.37 ± 0.03	0.88 ± 0.04
	$\perp (101)$	37.3	0.31 ± 0.02	0.85 ± 0.03
$\text{Bi}_{2.2}\text{Sr}_2\text{Ca}_{0.8}\text{Cu}_2\text{O}_{8+\delta}$ [35, 36]	$\parallel a, b$	10.0	0.48 ± 0.04	0.15 ± 0.02
	$\perp a, b$	30.0	0.16 ± 0.02	0.33 ± 0.05
$\beta\text{-FeSe}$ [37]	$\parallel (101)$	30.0	0.25 ± 0.06	0.68 ± 0.06
	$\perp (101)$	30.0	0.26 ± 0.02	0.70 ± 0.09
$\text{SmFeAsO}_{0.85}$ [39]	$\parallel c$	30.0	≈ 0.35	≈ 0.88
	$\perp (101)$	-	-	-

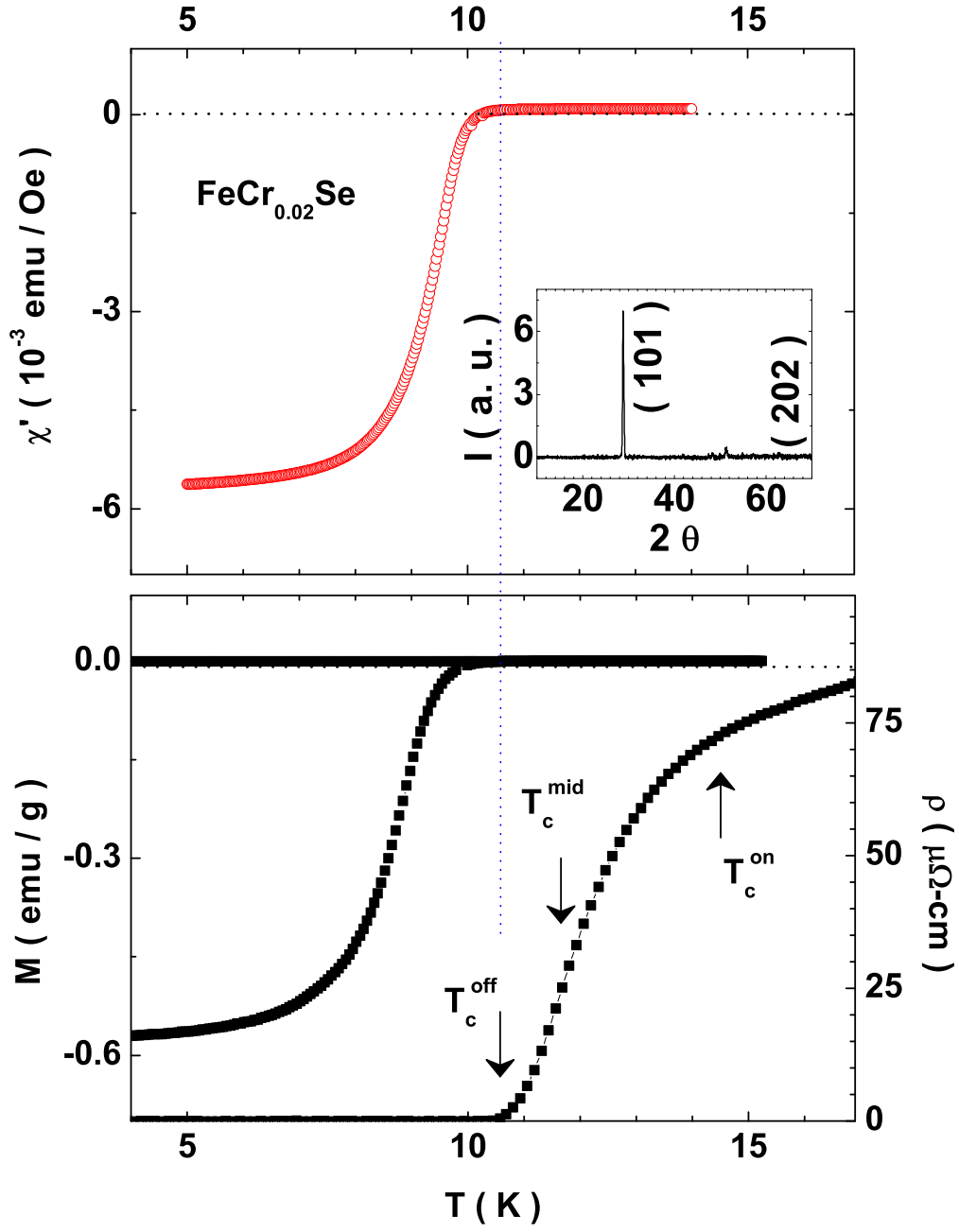


FIG. 1: (Color online) The x-ray diffraction pattern with identification of $(00l)$ lines for a cleaved piece of single crystal of $\text{FeSe}_{0.5}\text{Te}_{0.5}$ (see text for details).

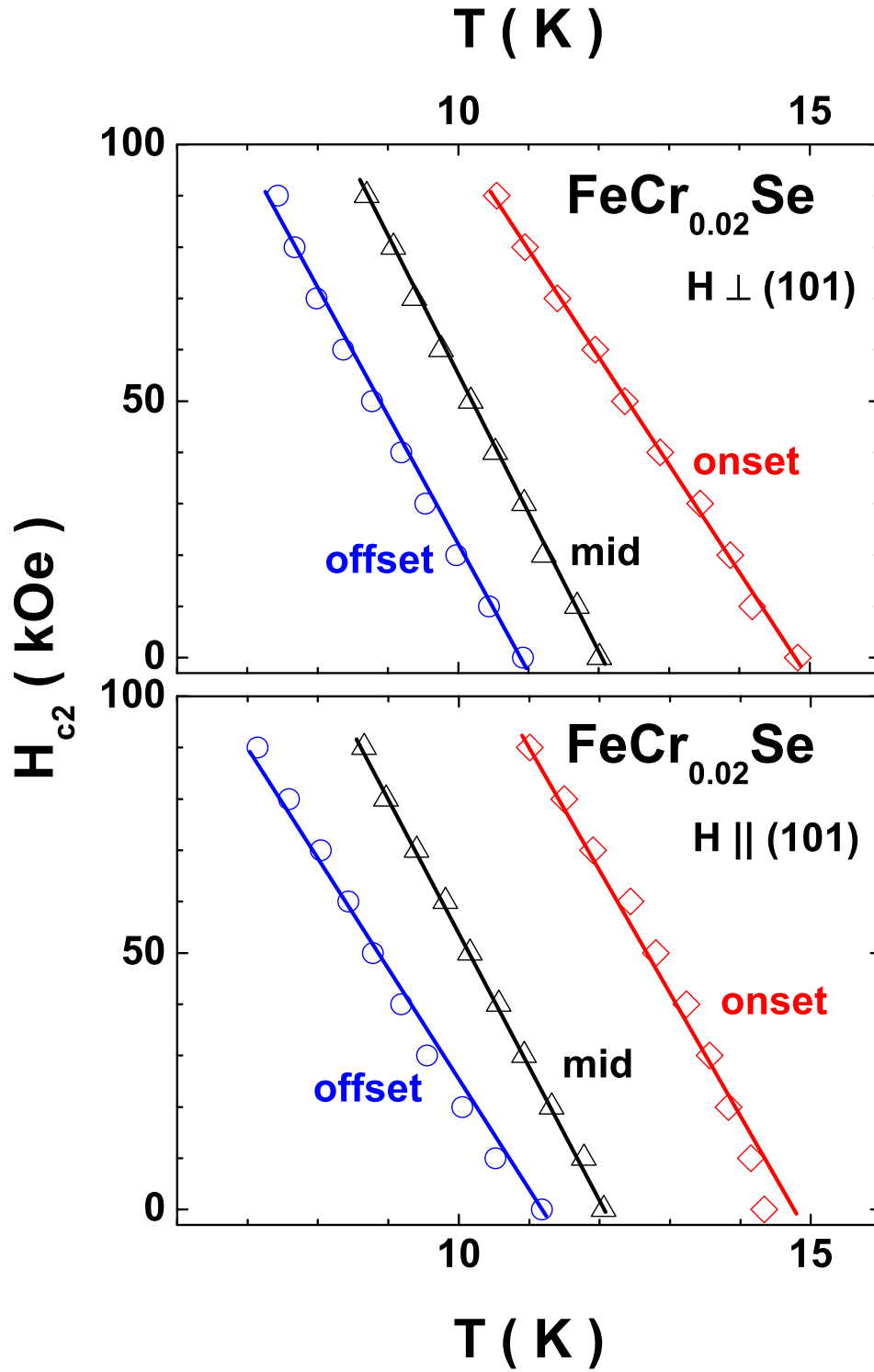


FIG. 2: (Color online) The upper critical field, $H_{c2}(T)$ obtained using different criteria (see text for details) for $H \parallel (101)$ (panel (a)) and $H \perp (101)$ (panel (b)).

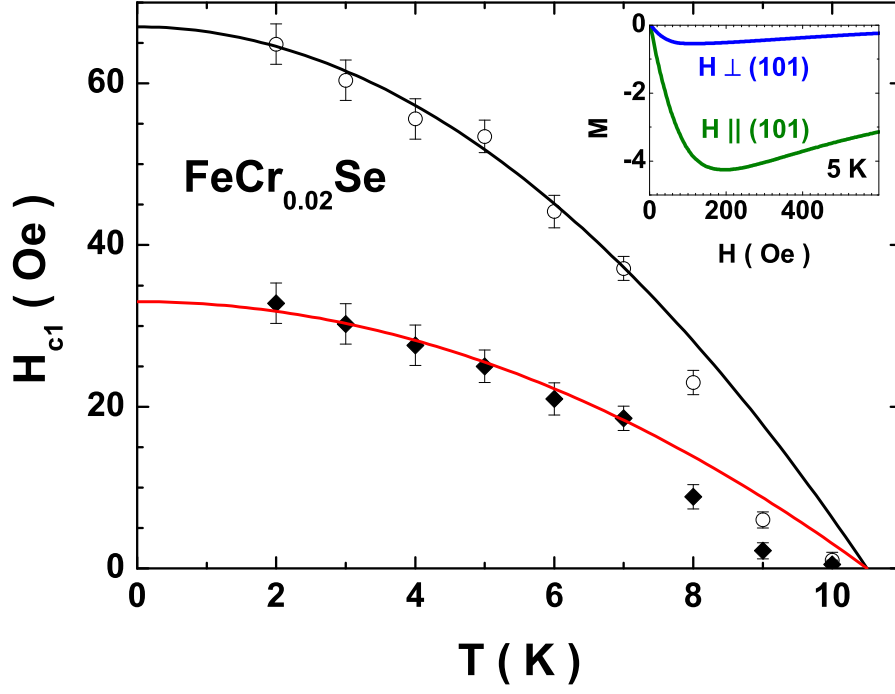


FIG. 3: (Color online) The lower critical field, $H_{c1}(T)$ obtained for both $H \parallel (101)$ and $H \perp (101)$. The inset panel shows a portion of the virgin isothermal M - H data for both $H \parallel (101)$ and $H \perp (101)$ obtained at 5 K.

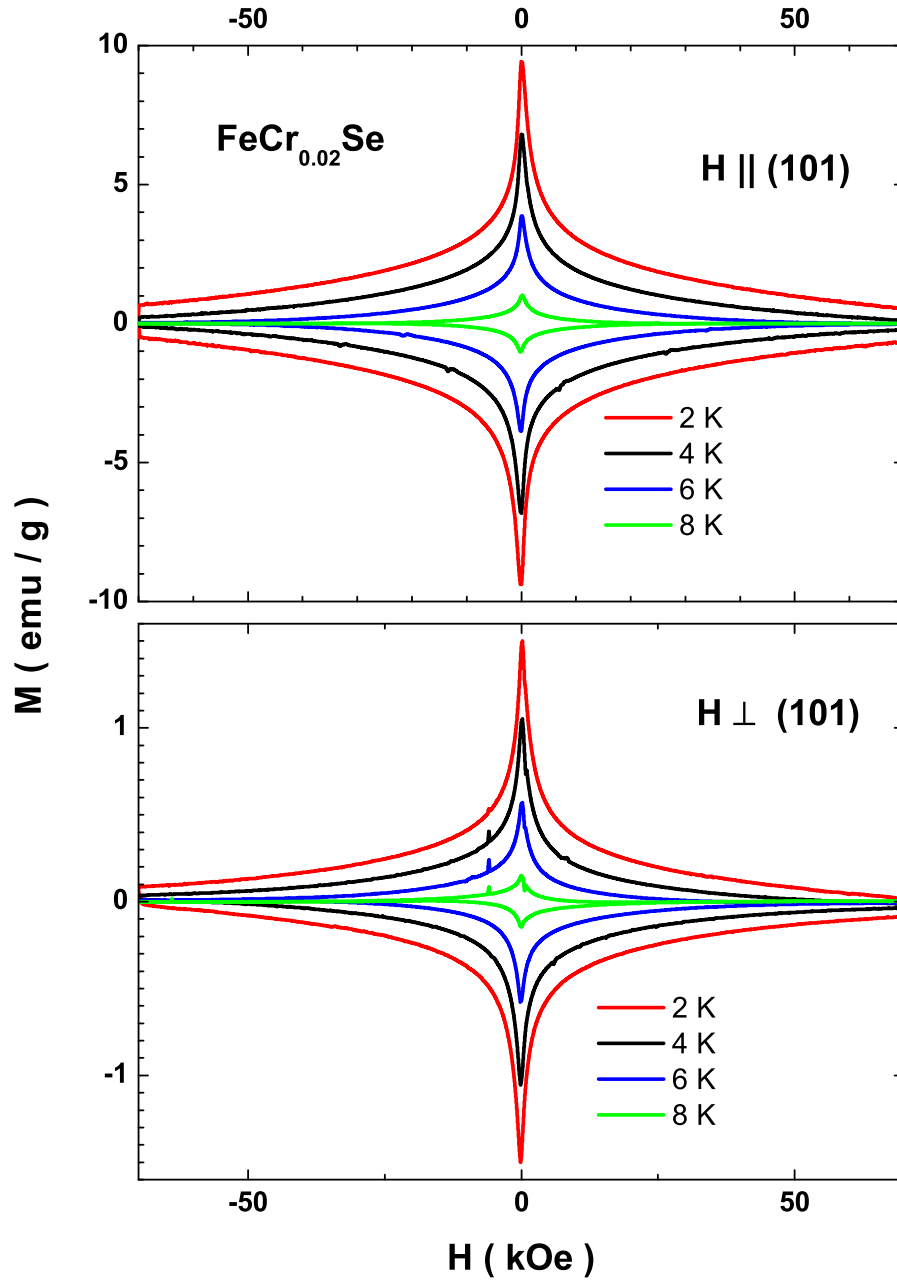


FIG. 4: (Color online) Isothermal magnetization (M – H) data obtained at various temperatures for $\text{H} \parallel (101)$ (panel (a)) and $\text{H} \perp (101)$ (panel (b))

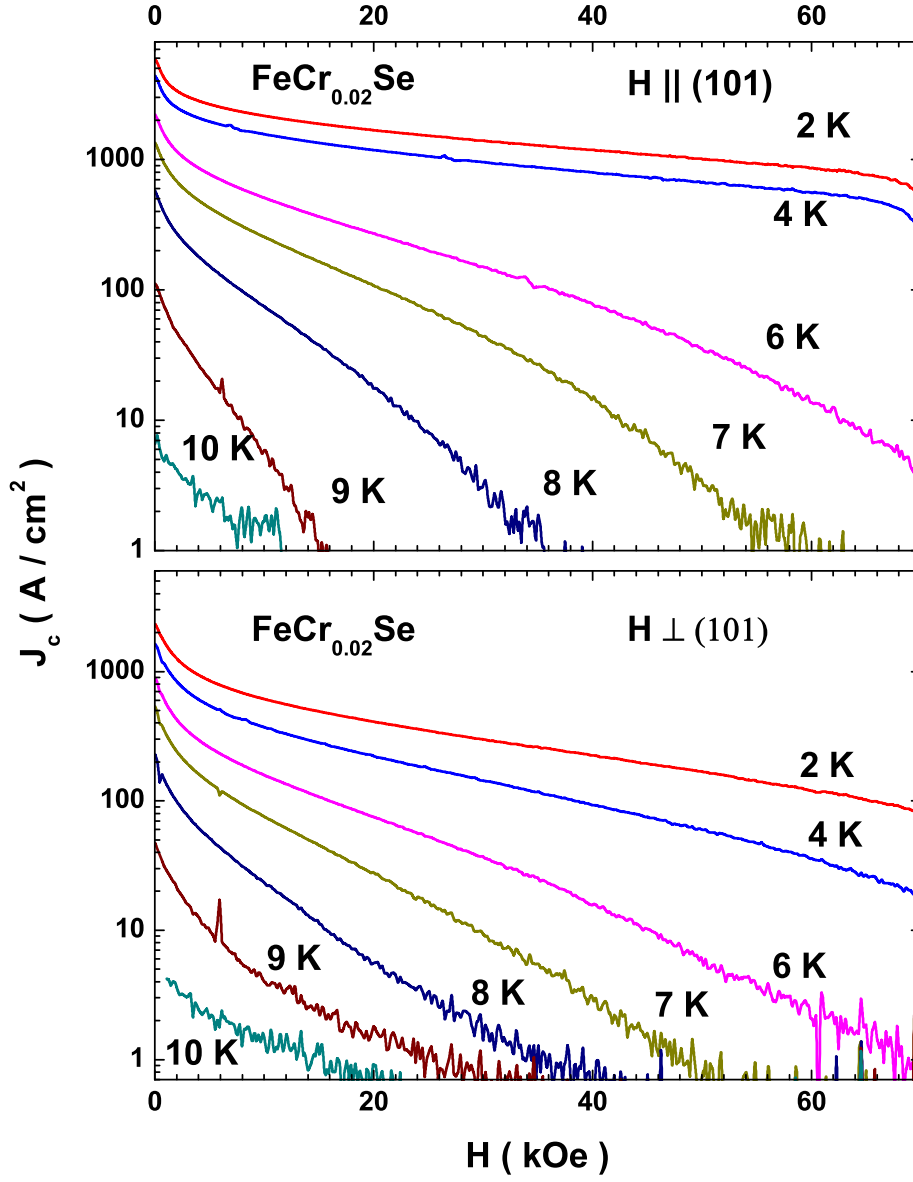


FIG. 5: (Color online) Critical current density ($J_c(H)$) data obtained at various temperatures for $H \parallel (101)$ (panel (a)) and $H \perp (101)$ (panel (b)).

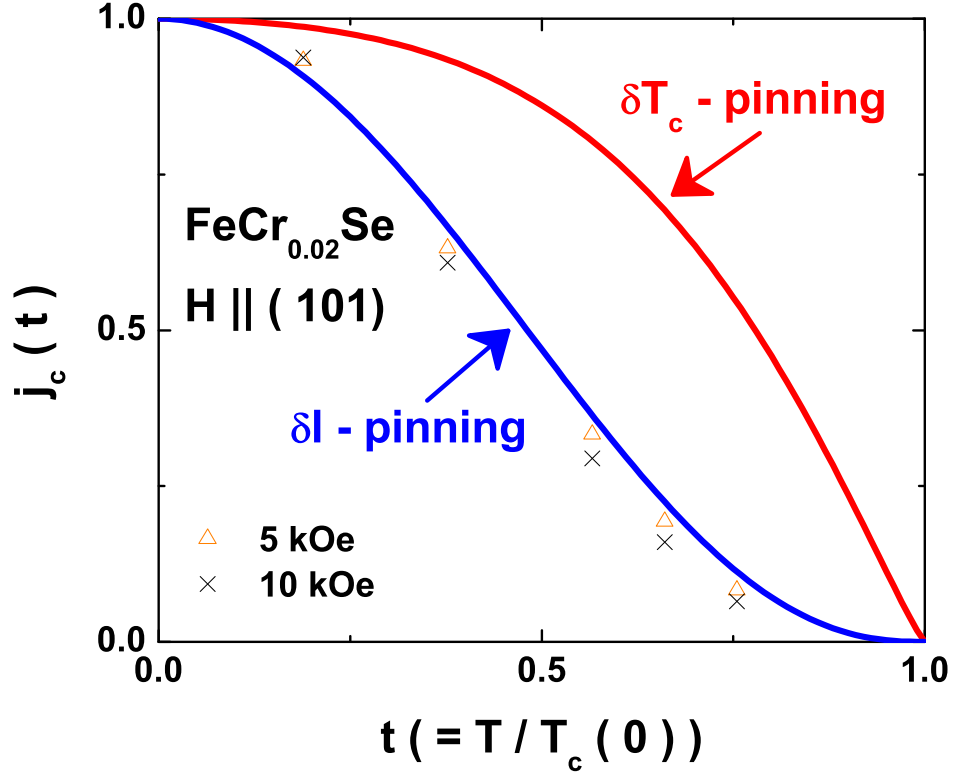


FIG. 6: (Color online) Theoretically expected variation of the normalized critical current density (J_c) with reduced temperature within the δl (solid black line) and δT_c (dotted red line). Also plotted are the experimentally obtained data points for (J_c) obtained at typical magnetic field strengths of 5 kOe and 10 kOe for H || (101).

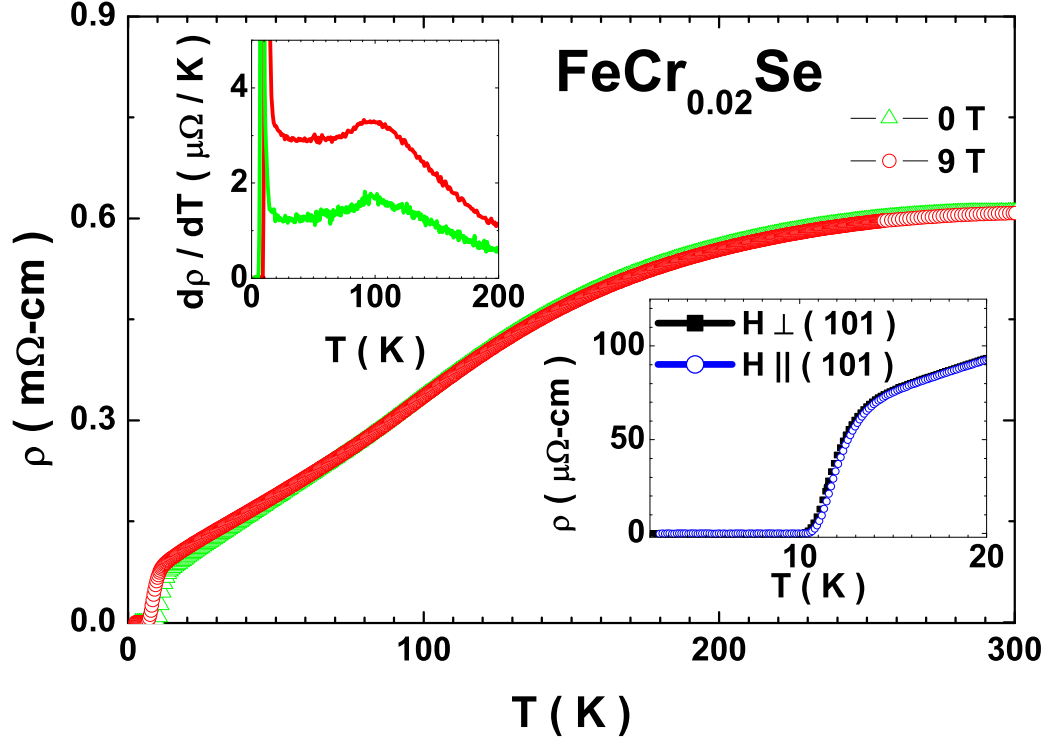


FIG. 7: (Color online) Variation of resistivity (ρ) as a function of temperature for a suitably cleaved single crystal of FeCr_xSe obtained in an external dc magnetic field of 0 T and 9 T, respectively for $H \parallel (101)$. Inset (a): Variation of $\frac{d\rho}{dT}$ with temperature. Inset (b): Variation of ρ as a function of temperature for $H \parallel (101)$ and $H \perp (101)$ respectively.

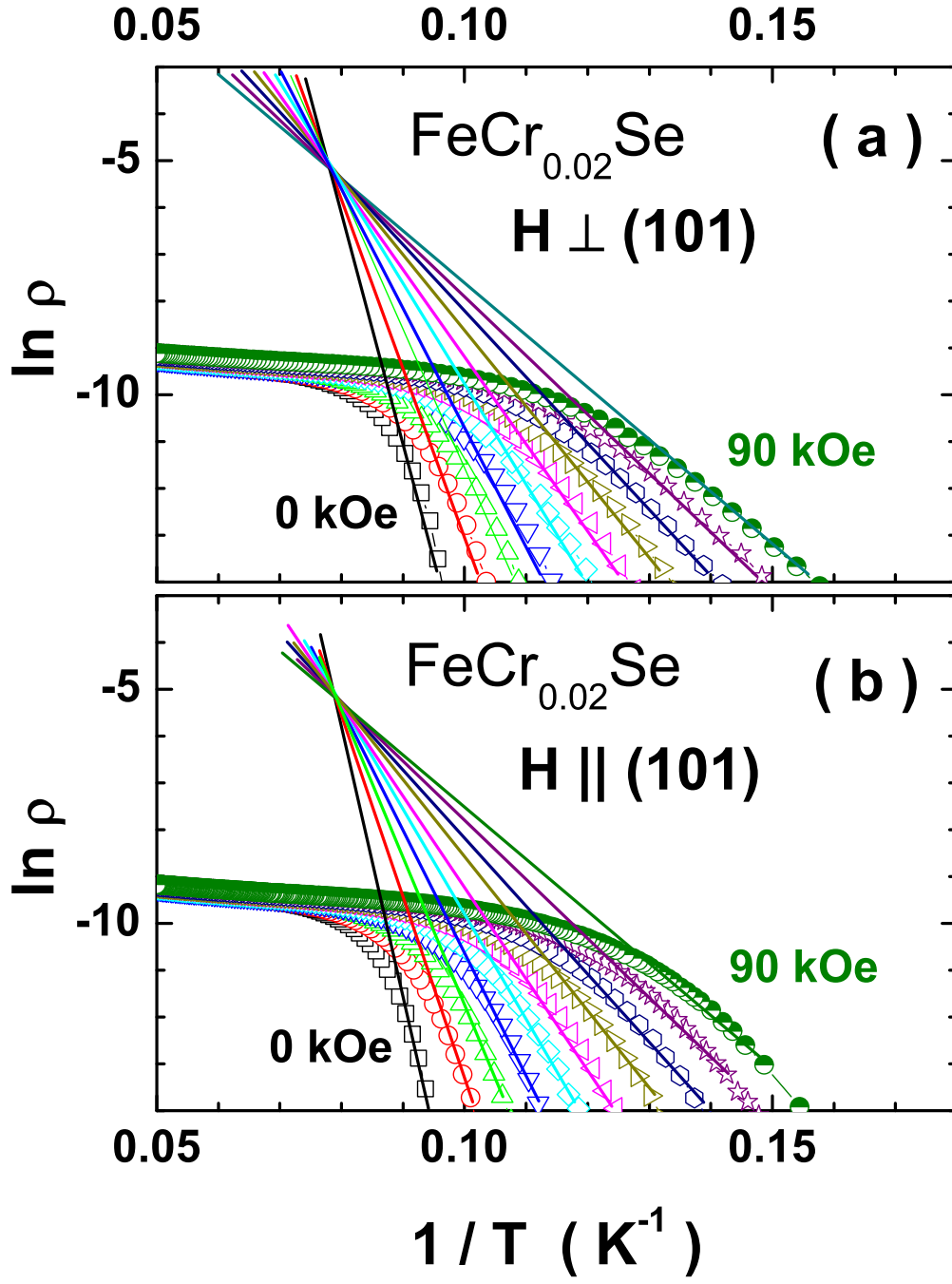


FIG. 8: (Color online) $\ln \rho$ versus $1/T$ at various externally applied field values for (a) $\text{H} \parallel (101)$ and (b) $\text{H} \perp (101)$.

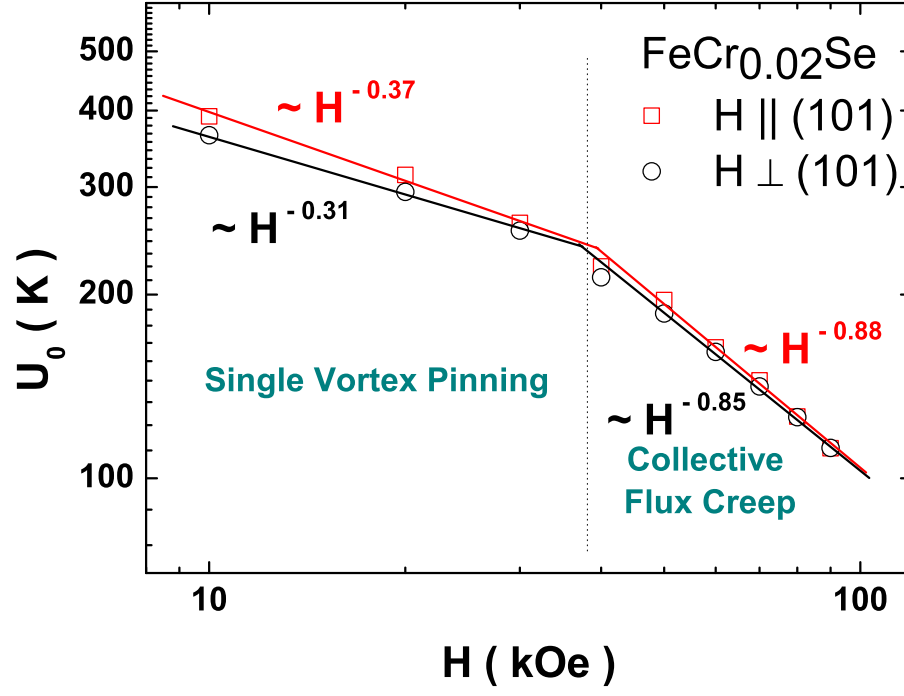


FIG. 9: (Color online) U_0 versus H for $H \parallel (101)$ and $H \perp (101)$. The power law fits are shown by bold lines.

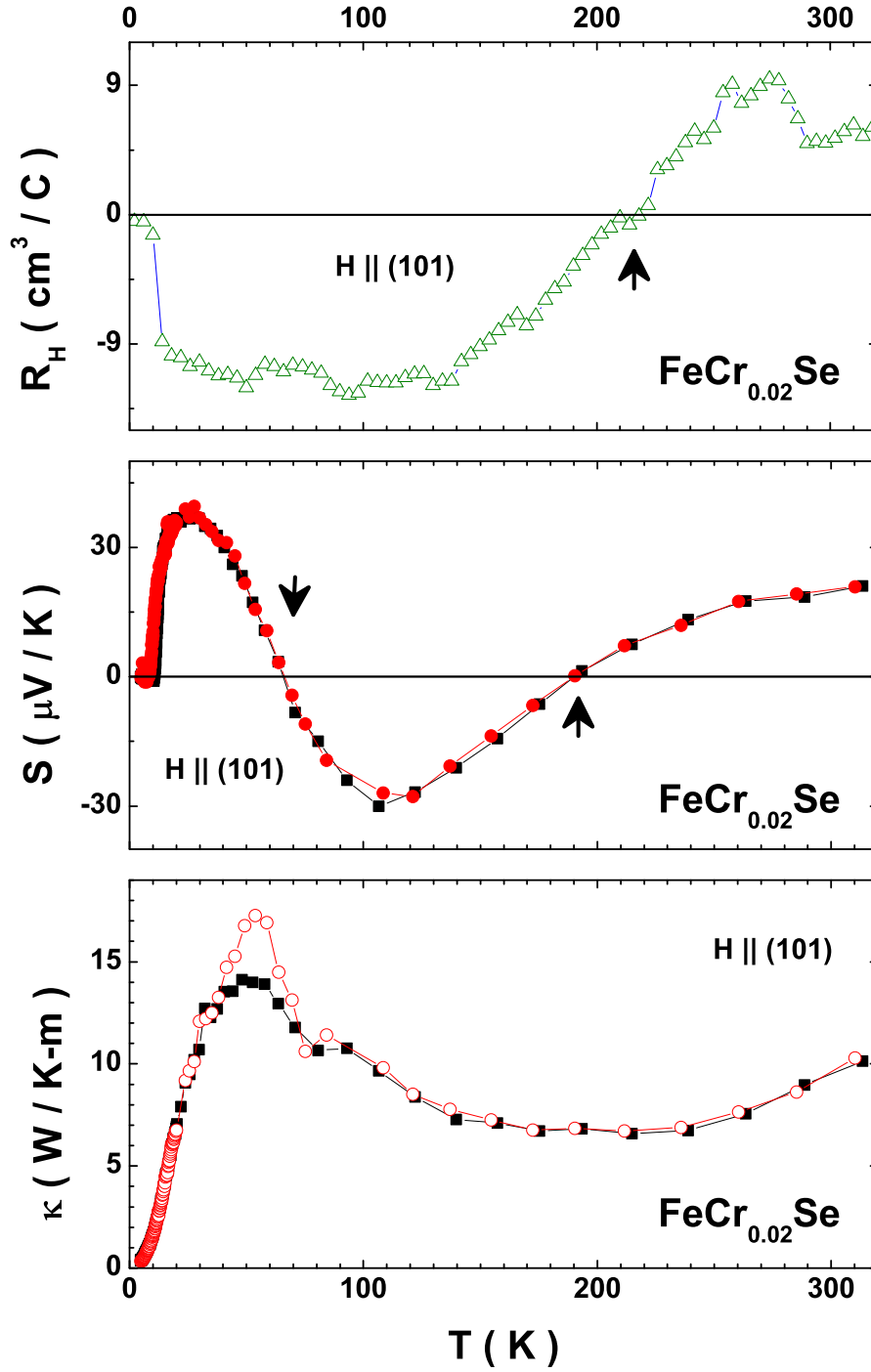


FIG. 10: (Color online) (a) Variation of Hall coefficient (R_H) with temperature of a suitably cleaved single crystal of FeCr_xSe (see text for details) in the presence of an external magnetic field of strength 5 T for $H \parallel (101)$. (b) Variation of thermopower (S) with temperature for a single crystal of FeCr_xSe at 0 T and 5 T, respectively for $H \parallel (101)$. Variation of S with temperature near T_c is shown as an inset in panel (b). (c) Variation of thermal conductivity (κ) with temperature